Appl. Phys. A 92, 381–385 (2008)
DOI: 10.1007/s00339-008-4535-x

Applied Physics A
Materials Science & Processing

F. CHEMAM[1,2,✉]
K. LENZ[2]
W. KUCH[2]

Influence of a Cr seed layer on the magnetic anisotropy of epitaxial Fe/Ag films on MgO(001)

[1] Laboratoire de Physique Appliquée et Théorique, Centre Universitaire de Tebessa, Algeria
[2] Institut für Experimentalphysik, Freie Universität Berlin, Arnimallee 14, 14195 Berlin, Germany

Received: 14 December 2007/Accepted: 3 April 2008
Published online: 20 May 2008 •

ABSTRACT The magnetic anisotropy of epitaxial 300 Å thick Fe films on Ag and Ag/Cr buffer layers on MgO(001) has been studied by ferromagnetic resonance and magneto-optic Kerr effect measurements. The samples were grown by molecular beam epitaxy at ambient temperature. A reduction of the effective magnetization for the samples with a Ag buffer layer is attributed to strain and dislocation formation as seen from X-ray diffraction measurements at low and high angles. In the samples with a Cr seed layer, a higher magnetic anisotropy is found which correlates with a reduced roughness.

PACS 75.50.Bb; 75.70.Cn; 76.50.+g; 68.35.Ct; 75.70.-i

1 Introduction

Thin magnetic films separated by non-magnetic spacer layers are widely investigated experimentally and theoretically because of their relevance for magneto-resistive applications. They show properties which differ considerably from those of the bulk, such as the magnetic anisotropy and interlayer exchange coupling. Fe/Ag multilayers have been extensively studied with respect to their physical properties, which depend on the surface and interface quality [1–7]. Ferromagnetic resonance (FMR) and magneto-optical Kerr effect (MOKE) show a reorientation transition of the magnetization from in-plane to out-of-plane at low Fe thickness, due to surface/interface anisotropy [8–12]. The structure of Ag thin films deposited on MgO(001) has been studied in a number of works [13–15]. It is established that the Ag thin films grow strained and form a square network of misfit dislocations at the interface with a periodicity of 10 nm, and that these dislocations are oriented along the ⟨110⟩ directions [13]. On the contrary, Fe and Cr thin layers grow perfectly on MgO(001) with much less strain than Ag [6, 7, 16]. However, Etienne et al. have shown that the growth of Fe on Ag gives rise to the formation of 3D islands, which in turn leads to a rough Fe surface [17]. Similar to that, thin Ag films on Fe layers on GaAs(001) tend to 3D-island growth, if they are below 100 nm thick, whereas flat Ag surfaces are obtained for Ag layers thicker than 200 nm [18]. Thus, using Cr as a seed layer on MgO(001) may be a promising alternative for Fe/Ag multilayers with thinner spacers.

Having this in mind, the studies of Fe/Ag and Fe/Ag/Cr thin film bilayers presented in the following are important (i) to understand how a Cr seed layer influences the structure and the magnetic anisotropy of these Fe/Ag bilayers deposited on single crystalline MgO(001) by molecular beam epitaxy, and (ii) to compare these properties to bilayers that have been prepared without a Cr layer on MgO(001). MgO(001) as substrate was chosen because it allows for epitaxial growth of Cr as well as Fe on it [16, 17, 19]. In order to evaluate the magnitude of the uniaxial in-plane anisotropy $K_{2\parallel}$ and fourfold anisotropy $K_{4\parallel}$ with and without Cr seed layer, we have performed angle-dependent FMR measurements in in-plane and polar configuration, as well as MOKE. The results are compared to structural and growth quality information obtained from X-ray diffraction at low and high angles.

2 Experimental details

The Fe/Ag bilayers were prepared at K.U. Leuven (Belgium) by molecular beam epitaxy (MBE) in ultrahigh vacuum (UHV) onto polished MgO(001) at room temperature. The MgO(001) substrate was cleaned by annealing at 600 °C for 20 min. in UHV prior to deposition. The Ag layer was evaporated with a deposition rate of 1 Å/s using a Knudsen cell. The Fe and Cr layers were evaporated by electron beam evaporation at a rate of 0.3 Å/s each. All samples were covered by a Ag protective layer of 20 Å thickness. The final sample structure is: 20 Å Ag/300 Å Fe/t_{Ag}/MgO(001), with t_{Ag} being the Ag buffer layer thickness of either 50, 100, or 150 Å. We refer to these samples as series A using the notation $\mathrm{A}_{t_{\mathrm{Ag}}}$ (e.g. A_{50}, A_{100}, or A_{150}). For comparison, one sample (A_0) without any Ag buffer and cap layer is included. The second sample series B contains a Cr buffer layer of 75 Å giving the structure: 20 Å Ag/300 Å Fe/t_{Ag}/75 Å Cr/MgO(001).

The XRD measurements were also carried out at K.U. Leuven using a 12 kW Rikagu DMax rotating anode diffractometer with Cu K_α radiation ($\lambda = 1.5418$ Å) and a thin film attachment goniometer with a post-sample graphite(0002) crystal monochromator in Bragg–Brentano configuration. The room temperature magnetic properties were determined at the Freie Universität Berlin from angle dependent FMR measurements

✉ Fax: +213-37-49-92-00, E-mail: f.chemam@mail.univ-tebessa.dz

using a Varian spectrometer with a conventional microwave cavity setup at 9.2 GHz, and by MOKE at K.U. Leuven.

3 Results and discussion

The crystallographic orientation of the layers for series A samples is $[100]_{MgO} \parallel [100]_{Ag} \parallel [110]_{Fe}$, i.e., the Fe(001) lattice is rotated by 45° with respect to the Ag(001) lattice. The growth of the Ag layer on MgO(001) is island-like, as no RHEED oscillations are visible during evaporation [20]. The relationship of the sample series B with the Cr buffer layer is $[100]_{MgO} \parallel [110]_{Cr} \parallel [100]_{Ag} \parallel [110]_{Fe}$. The Cr lattice is azimuthally rotated by 45° with respect to the MgO(001) substrate [16]. The lattice mismatch between Ag and Cr is then only 2%, and the Ag layer is rotated by 45° with respect to both the Cr and Fe layer. As the surface energy of Cr (2400 mJ/m^2) is about twice that of Ag (1250 mJ/m^2) [17, 19], a Ag layer on the Cr buffer layer may improve the growth of thin films.

Figure 1 shows the low angle X-ray diffraction of three samples with and without the Cr buffer. Data for one sample of each series A and B with $t_{Ag} = 150$ Å, and the Fe reference sample A_0, i.e. without the Cr buffer and Ag layer, are presented. (The dataset for A_0 is the same as presented in [21, 22].) For sample B_{150} and A_0 interference fringes are visible, whereas for sample A_{150}, in which the Ag layer is in direct contact with the MgO substrate, no fringes are observable. The absence of fringes can be explained by a higher surface roughness, or by the formation of a dislocation network. Additionally one can see that for sample B_{150} and A_0 the interference fringe intensity decreases with increasing scattering vector, which is caused by interface roughness [23]. The distinctly higher decay rate of the reflected intensity for sample A_0 results from some surface roughness [23] not observed that strongly for samples A_{150} and B_{150}. This behavior is representative also for the other samples of the same series.

The corresponding high angle X-ray diffraction data of the same three samples is given in Fig. 2. At $2\theta = 42.9°$ ($Q = 2.98$ Å^{-1}) the MgO(002) peak is observed. The Ag(002), Cr(002), and Fe(002) peaks appear at angles $2\theta = 44.5°$ ($Q = 3.10$ Å^{-1}), $2\theta = 64.6°$ ($Q = 4.36$ Å^{-1}), and $2\theta = 65.6°$ ($Q = 4.43$ Å^{-1}), respectively, which indicates that all samples are epitaxial. A forbidden MgO(003) peak at $Q = 4.50$ Å^{-1} appears only for sample A_{150} (without the Cr layer) and may be due to growth induced strain, dislocations, or substrate quality [24, 25]. For sample B_{150} the intensities of the Ag(002) and Fe(002) peaks are higher than those of sample A_{150}. From this low and high angle XRD data, it follows that the interface and surface roughness of a Fe/Ag stack directly grown on MgO(001) can be reduced using a Cr buffer layer of 75 Å, improving the epitaxial quality.

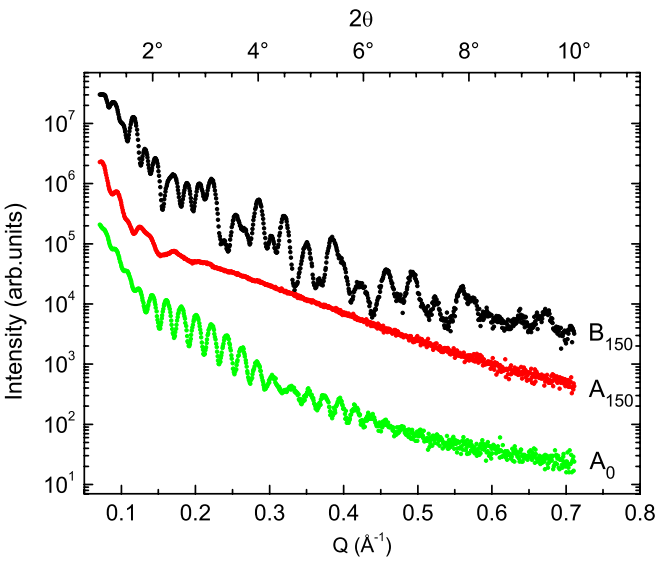

FIGURE 1 Low angle X-ray diffraction curves of samples A_{150}, B_{150}, and the reference sample A_0. The *curves* are vertically offset for better visibility

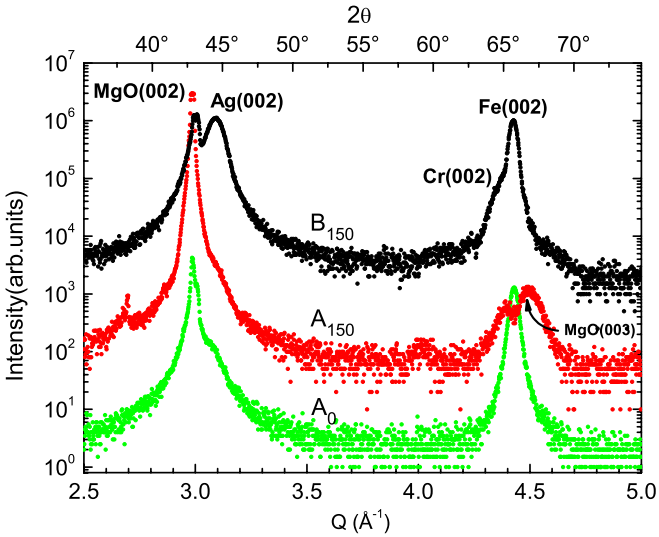

FIGURE 2 High angle X-ray diffraction curves of samples A_{150}, B_{150}, and the reference sample A_0. The curves are vertically offset for visibility

For the determination of the magnetic anisotropy we use the following definition of the magnetic part of the free energy density for cubic symmetry [26]:

$$F = -\boldsymbol{M}\cdot\boldsymbol{H} - \left(K_{2\perp} - 2\pi M^2\right)\cos^2\theta + K_{2\parallel}\sin^2\theta\cos^2(\varphi-\varphi_u) + K_4\sin^2\theta - \frac{1}{8}K_4(7+\cos 4\varphi)\sin^4\theta\,, \quad (1)$$

where $\boldsymbol{M}$ is the magnetization, and $\boldsymbol{H}$ is the external magnetic field. θ denotes the angle between $\boldsymbol{M}$ and the film normal, φ the in-plane angle between $\boldsymbol{M}$ and the [100] direction of Fe, and φ_u is the angle of the easy axis of the uniaxial in-plane anisotropy $K_{2\parallel}$ with respect to the easy axis of the fourfold anisotropy K_4.

Using the general approach of Smit and Beljers [27], the resonance conditions for out-of-plane $H_{res}(\theta_H)$ or in-plane $H_{res}(\varphi_H)$ field angle-dependent ferromagnetic resonance measurements can be derived from (1), see, e.g. [28] for details. For the polar angular dependence in which $\boldsymbol{H}$ is varied between the [110] and the [001] direction follows:

$$\left(\frac{\omega}{\gamma}\right)^2 = \left\{H_{res}\cos\Delta\theta + \frac{3K_4}{2M}\cos 4\theta_{eq} + \left[-4\pi M_{eff} + \frac{K_4}{2M} + \frac{2K_{2\parallel}}{M}\cos^2\left(\frac{\pi}{4}+\varphi_u\right)\right]\cos 2\theta_{eq}\right\}$$

$$\times \left\{ H_{\mathrm{res}} \cos\Delta\theta + \frac{3K_4}{M}\cos^4\theta_{\mathrm{eq}} + \left[-4\pi M_{\mathrm{eff}} + \frac{K_4}{M} + \frac{2K_{2\parallel}}{M}\cos^2\left(\frac{\pi}{4}+\varphi_{\mathrm{u}}\right)\right]\cos^2\theta_{\mathrm{eq}} - \frac{2K_4}{M} + \frac{2K_{2\parallel}}{M}\sin 2\varphi_{\mathrm{u}} \right\} - \left[\frac{K_{2\parallel}}{M}\cos\theta_{\mathrm{eq}}\cos 2\varphi_{\mathrm{u}} \right]^2, \quad (2)$$

where $\Delta\theta = \theta_{\mathrm{eq}} - \theta_{\mathrm{H}}$ with θ_{eq} being the equilibrium polar angle of $\boldsymbol{M}$. For the azimuthal angular dependence ($\theta_{\mathrm{H}} = 90°$) follows:

$$\left(\frac{\omega}{\gamma}\right)^2 = \left\{ H_{\mathrm{res}}\cos\Delta\varphi + 4\pi M_{\mathrm{eff}} + \frac{K_4}{2M}\left[3+\cos 4\varphi_{\mathrm{eq}}\right] + \frac{2K_{2\parallel}}{M}\cos^2\left(\varphi_{\mathrm{eq}}-\varphi_{\mathrm{u}}\right)\right\} \times \left\{ H_{\mathrm{res}}\cos\Delta\varphi + \frac{2K_4}{M}\cos 4\varphi_{\mathrm{eq}} + \frac{2K_{2\parallel}}{M}\cos 2\left(\varphi_{\mathrm{eq}}-\varphi_{\mathrm{u}}\right)\right\}, \quad (3)$$

where $\Delta\varphi = \varphi_{\mathrm{eq}} - \varphi_{\mathrm{H}}$ with φ_{eq} being the equilibrium azimuth angle of $\boldsymbol{M}$. The fit of the angle-dependent data with (2) and (3) results in the anisotropy fields $K_{2\parallel}/M$ and K_4/M, as well as in the effective magnetization $4\pi M_{\mathrm{eff}} = 4\pi M - 2K_{2\perp}/M$.

The FMR in-plane angular dependence taken at 9.24 GHz and room temperature for samples A_{150} and B_{150} is shown in Fig. 3. The in-plane angle of the external magnetic field φ_{H} was varied between $-110°$ and $+70°$. The solids lines are fits to the resonance condition using the parameters presented in Table 1. Sample A_{150} exhibits only one resonance per field angle (squares), whereas for sample B_{150} with Cr buffer (circles), two resonances are observable. These are the so-called saturated (solid circles) and the unsaturated resonance modes (open circles), respectively. The saturated resonance mode corresponds to the (uniform) precession of $\boldsymbol{M}$ around $\boldsymbol{H}$ in a sample magnetically saturated by the external field. If the external field is smaller than the internal anisotropy fields, $\boldsymbol{M}$ precesses around the direction of the internal field, resulting in the unsaturated mode [26, 29]. To determine the magnetic anisotropy we used only the saturated mode for fitting. Due to a comparatively high anisotropy of sample B_{150}, the resonance modes are observable only in a narrow range of about 10° around the Fe ⟨110⟩ directions, which are the hard axes in the film plane. Therefore, the easy axis resonances of sample B_{150} cannot be excited, because no solution fulfilling the resonance equation (3) exists for these field directions. The same was observed for all samples of series B. Similar resonance modes have been observed at 9 GHz in Fe/MgO(001) [30, 31] and Fe/GaAs [26, 32], for example. Sample A_{150} also shows a clear fourfold anisotropy, and the resonances can be found over the whole range of in-plane angles. Minima of the resonance field are found along the in-plane ⟨100⟩ directions, which are thus the easy axes for both series of samples. The ⟨110⟩ in-plane directions thus are the intermediate (hard in-plane) axes of the films. The film's normal is the hard axis due to the shape anisotropy of the thin films.

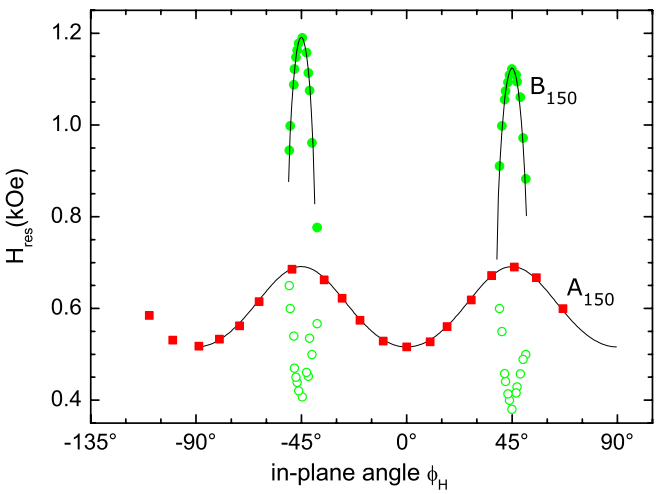

FIGURE 3 In-plane angular dependence of H_{res} for samples A_{150} (*red squares*) and B_{150} (*green circles*). The *open circles* denote the resonance field of the unsaturated mode of sample B_{150}. The *solid lines* are the fits as described in the text

Sample	$4\pi M_{\mathrm{eff}}$ (kOe)	$K_{2\parallel}/M$ (Oe)	K_4/M (Oe)	K_4^{MOKE}/M (Oe)	H_{c} (Oe)
A_0	–	–	–	–355(40)	2.0(3)
A_{50}	–11.1(2)	0	–36(2)	–28(8)	58(1)
A_{100}	–11.0(2)	0	–40(2)	–81(8)	66(1)
A_{150}	–16.0(1)	0	–45(2)	–52(8)	48(1)
B_{50}	–18.8(2)	–15(1)	–260(2)	–376(40)	5.4(3)
B_{100}	–17.8(2)	–17(1)	–275(2)	–262(40)	8.5(3)
B_{150}	–17.8(2)	–17(1)	–285(2)	–327(40)	5.1(3)

TABLE 1 Effective magnetization, uniaxial and fourfold magnetic anisotropy fields, and the coercivity along the [100] easy axis of the samples from series A (without Cr) and B (with Cr)

Figure 4 shows the corresponding polar angular dependence of the two samples with $t_{\mathrm{Ag}} = 150$ Å. The external field is rotated from the film's normal ($\theta_{\mathrm{H}} = 0°$) into the film plane pointing then along the [110] direction ($\theta_{\mathrm{H}} = 90°$, $\varphi_{\mathrm{H}} = 45°$). Again, for the B-type sample the saturated and unsaturated resonance modes are visible (solid and open circles), whereas for the A-type sample only the saturated branch exists (squares). From the polar angular dependence shown in Fig. 4, the effective magnetization $4\pi M_{\mathrm{eff}}$ is determined, which is roughly 40% higher for the series B samples than for series A.

The results for all six samples are summarized in Table 1. The effective magnetization of series B of 17.8–18.8 kOe is in good agreement with the bulk value of Fe and the work of Chemam et al. on [Ag/Fe]/MgO(001) superlattices [33]. The effective magnetization of series A is 38% smaller. The values of the fourfold anisotropy field $K_4/M = 285$ Oe and the uniaxial in-plane anisotropy field $K_{2\parallel} = 17$ Oe of the sample B_{150} with the Cr buffer deduced from the fits of Figures 3 and 4 are in good agreement with the Fe bulk value and the values reported by Zakeri et al. for Fe/GaAs [28]. However, the origin of the small in-plane uniaxial anisotropy found in series B but not in series A remains unclear. It might be due to uniaxial stress within the Fe film or (at least) at the Fe/Ag interface, induced by the underlying Cr buffer.

Compared to series B, the values of the fourfold anisotropy field in the series A samples are smaller by a factor of about

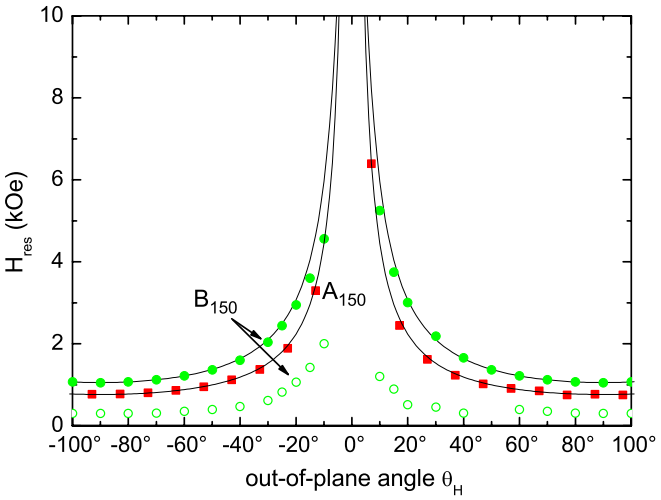

FIGURE 4 Polar angular dependence of H_{res} for the samples with $t_{Ag} = 150$ Å. *Red squares* denote the sample A_{150} without the Cr buffer and *solid (open) green circles* refer to the saturated (unsaturated) mode of sample B_{150}. The *solid lines* are fits as described in the text

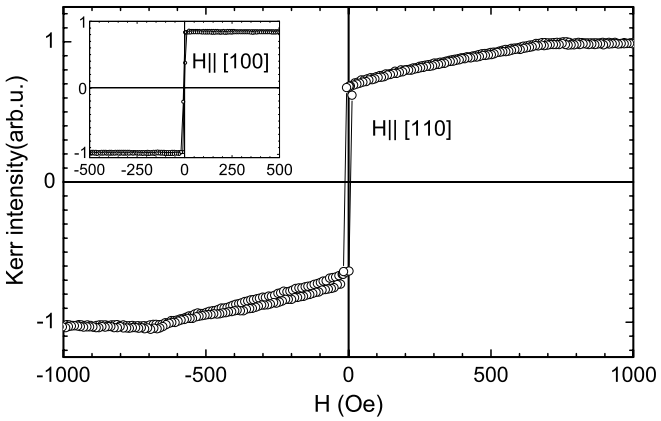

FIGURE 5 MOKE hysteresis loops of sample A_0 measured along the [110] intermediate direction. The *inset* shows the hysteresis loop for the [100] easy axis

7, which is attributed to the formation of dislocations and strain at the Ag/MgO(001) interface and reduced epitaxial quality. A similar case of reduced magnetic anisotropy was observed in Fe/GaAs [34, 35], which was attributed to the lattice mismatch at the interface or even the existence of inhomogeneities due to crystal imperfections, which may appear during the growth process.

Figure 5 shows MOKE hysteresis loops of sample A_0 for the magnetic field applied along the intermediate [110] axis and also along the easy axis [100]. It can be seen that when the field is applied along the [110] direction, there is an almost linear decrease of the magnetization from saturation to a remanence of 68% as the field strength is reduced. After compensating the coercive field of 6.8 Oe an abrupt jump followed by a further linear decrease occurs until negative saturation is reached. This jump is caused by the nucleation of domains with magnetization along the opposite easy [0−10] direction and the rapid movement of domain walls across the sample. The slow increase in Kerr intensity reflects the subsequent rotation of the moments into the [−1 − 10] intermediate direction. In contrast, along the [100] direction (see inset in Fig. 5), one observes a square-like hysteresis loop with a coercivity of only 2.0 Oe [36, 37].

For all samples the fourfold anisotropy field K_4/M was estimated from the area between intermediate and easy axis hysteresis curves and given as K_4^{MOKE} in Table 1. The results show the same order of magnitude as the FMR results. Note that the fourfold anisotropy of series B is comparable to that of the pure Fe film (sample A_0) or to Fe films prepared by ion-beam sputter epitaxy [38].

The last column of Table 1 contains the coercivity H_c along the easy axis. For series A, H_c is one order of magnitude higher than for series B. In principle, the coercivity H_c is affected by two mechanisms: (i) the nucleation and domain wall motion determining the magnetization reversal process and (ii) the surface roughness or formation of dislocations, i.e. disorder in the magnetic system hindering the propagation of reversed domains. In our case it is probably the second one, i.e. in series A the formation of dislocations during growth increases the coercive field. A similar behavior of H_c due to dislocation formation was found in Fe/W(100) [39].

4 Conclusion

In conclusion, by FMR we investigated the influence of a Cr seed layer on the magnetic anisotropy of Fe/Ag thin films on MgO(001). The easy and intermediate magnetization axes were found to be the ⟨100⟩ and ⟨110⟩ in-plane directions of Fe, respectively. From the FMR analysis we obtained the effective magnetization, the in-plane uniaxial and fourfold anisotropy fields. The growth of Fe/Ag bilayers (and probably [Ag/Fe] superlattices) on MgO(001) substrates is improved significantly by insertion of a Cr seed layer on the MgO substrate, leading to magnetic properties of the Fe layer similar to that of single-crystalline Fe films. This is confirmed by X-ray diffraction measurements. For the samples without the Cr buffer layer (series A), the reduction of the effective magnetization and fourfold anisotropy field is attributed to the formation of strain and dislocations at the substrate's interface.

ACKNOWLEDGEMENTS The Algerian Ministry of Higher Education and Scientific Research and the Tebessa university are acknowledged for supporting F.C.'s stay in Berlin. We would like to thank Y. Bryunseraede and K. Temst of K.U. Leuven (Belgium) for providing the samples and for help with the XRD measurements.

REFERENCES

1 G. Gladyszewski, K. Temst, K. Mae, R. Schad, F. Beliën, E. Kunnen, G. Verbanck, Y. Bruynseraede, R. Moons, A. Vantomme, S. Blässer, G. Langouche, Thin Solid Films **366**, 51 (2000)
2 A. Tunyogi, F. Paszti, Z. Osvath, F. Tanczikó, M. Major, E. Szilagyi, Nucl. Instrum. Methods Phys. Res. B **249**, 384 (2006)
3 T. Phalet, M.J. Prandolini, W.D. Brewer, P. Schuurmans, N. Severijns, B.G. Turrell, B. Vereecke, S. Versyck, Phys. Rev. B **71**, 144431 (2005)
4 A. Hahlin, C. Andersson. J. Hunter-Dunn, B. Sanyal, O. Karis, D. Arvanitis, Phys. Rev. B **73**, 134423 (2006)
5 X.Y. Li, L.T. Kong, B.X. Liu, Phys. Rev. B **72**, 054118 (2005)
6 F. Chemam, A. Bouabellou, R. Halimi, Thin Solid Films **380**, 266 (2000)
7 F. Chemam, A. Bouabellou, R. Halimi, M.-F. Mosbah, J. Magn. Magn. Mater. **211**, 320 (2000)
8 D.P. Pappas, C.R. Brundle, H. Hopster, Phys. Rev. B **45**, 8169 (1992)
9 Z.Q. Qiu, J. Pearson, S.D. Bader, Phys. Rev. Lett. **70**, 1006 (1993)
10 D.M. Schaller, D.E. Bürgler, C.M. Schmidt, F. Meisinger, H.-J. Güntherodt, Phys. Rev. B **59**, 14516 (1999)

11 B. Heinrich, K.B. Urquhart, A.S. Arrot, J.F. Cochran, K. Myrtle, S.T. Purcell, Phys. Rev. Lett. **59**, 1756 (1987)
12 R. Cabanel, P. Etienne, S. Lequien, G. Creuzet, A. Berthelemy, A. Fert, J. Appl. Phys. **67**, 5243 (1997)
13 A. Ouahab, C. Mottet, J. Goniakowski, Phys. Rev. B **72**, 035 421 (2005)
14 P. Guenard, G. Renaud, B. Villette, Physica B **221**, 205 (1996)
15 O. Robach, G. Renaud, A. Barbier, Phys. Rev. B **60**, 5858 (1999)
16 E. Kunnen, S. Mangin, V.V. Moshchalkov, Y. Bruynseraede, A. Vantomme, A. Hoser, K. Temst, Thin Solid Films **414**, 262 (2002)
17 P. Etienne, J. Mascis, J. Phys. III **3**, 1581 (1991)
18 J. Lösch, P. Leinenbach, U. Memmert, U. Hartmann, Appl. Phys. A **66**, S1133 (1998)
19 S. Demuynck, J. Meersschaut, J. Dekoster, B. Swinnen, R. Moons, A. Vantomme, S. Cottenier, M. Rots, Phys. Rev. Lett. **81**, 2562 (1998)
20 F. Petroff, Multicouches magnétiques Fe/Ag, Fe/Cr, Co/Cu, Fe/Cu: de l'élaboration aux propriétés magnétiques et électronique, PhD-thesis, Paris-Sud University (1992)
21 F. Chemam, R. Boukhalfa, A. Bouabellou, Phys. Stat. Solidi C **3**, 1298 (2006)
22 F. Chemam, A. Bouabellou, R. Boukhalfa, J. Magn. Magn. Mater. **272–276**, 1174 (2004)
23 J.M. Baribeau, Appl. Phys. Lett. **57**, 1748 (1990)
24 Q. Li, Y. Yu, G. Singh Bhatia, L.D. Marks, S.C. Lee, Y.W. Chung, J. Vac. Sci. Technol. A **18**, 2333 (2000)
25 V.K. Kiselev, S.V. Obolenskii, V.D. Skupov, Tech. Phys. **44**, 724 (1999)
26 K. Zakeri, T. Kebe, J. Lindner, M. Farle, J. Magn. Magn. Mater. **299**, L1 (2006)
27 J. Smit, H.G. Beljers, Philips. Res. Rep. **10**, 133 (1955)
28 K. Lenz, E. Kosubek, K. Baberschke, H. Wende, J. Herfort, H.-P. Schönherr, K.H. Ploog, Phys. Rev. B **72**, 144 411 (2005)
29 K. Lenz, E. Kosubek, K. Baberschke, J. Herfort, H.-P. Schönherr, K.H. Ploog, Phys. Stat. Solidi **3**, 122 (2006)
30 Y.V. Goryunov, N.N. Garif'yanov, G.G. Khaliullin, I.A. Garifullin, L.R. Tagirov, F. Schreiber, T. Mühge, H. Zabel, Phys. Rev. B **52**, 13 450 (1995)
31 P. Poulopoulos, P. Isberg, W. Platow, W. Wisny, M. Farle, B. Hjörvarsson, K. Baberschke, J. Magn. Magn. Mater. **170**, 57 (1997)
32 M. Doi, B. Roldan Cuenya, W. Keune, T. Schmitte, A. Nefedov, H. Zabel, D. Spoddig, R. Meckenstock, J. Pelzl, J. Magn. Magn. Mater. **240**, 407 (2002)
33 F. Chemam, A. Bouabellou, A. Layadi, S. Senoussi, Mater. Sci. Eng. C **19**, 125 (2002)
34 E.C. Silva, R. Meckenstock, O. Geisau, R. Kordecki, J. Pelzl, J.A. Wolf, P. Grünberg, J. Magn. Magn. Mater. **121**, 528 (1993)
35 Y. Zai, L. Shi, W. Zhang, Y.X. Xu, M. Lu, H.R. Zhai, W.X. Tang, X.F. Jin, Y.B. Xu, J.A.C. Bland, Appl. Phys. Lett. **93**, 7622 (2003)
36 K. Postava, H. Jaffres, A. Schuhl, F. Nguyen Van Dau, M. Goiran, A.R. Fert, J. Magn. Magn. Mater. **172**, 199 (1997)
37 E. Gu, J.A.C. Bland, C. Daboo, M. Gester, L.M. Brown, R. Ploessl, J.N. Chapman, Phys. Rev. B **51**, 3596 (1995)
38 T. Damm, M. Buchmeier, A. Schindler, D.E. Bürgler, P. Grünberg, C.M. Schneider, J. Appl. Phys. **99**, 093 905 (2006)
39 W. Wulfhekel, F. Zavaliche, F. Porrati, H.P. Oepen, J. Kirschner, Eur. Phys. Lett. **49**, 651 (2000)